RIP3-mediated necrotic cell death accelerates systematic inflammation and mortality

Lingjun Meng[a,b], Wei Jin[c], and Xiaodong Wang[a,1]

[a]National Institute of Biological Sciences, Beijing 102206, China; [b]College of Biological Sciences, China Agricultural University, Beijing 100094, China; and [c]Institute For Immunology, Tsinghua University, Beijing 100084, China

Contributed by Xiaodong Wang, July 29, 2015 (sent for review July 13, 2015; reviewed by Guosheng Liang)

Systematic inflammation contributes to the development of many diseases, including cardiovascular disease, which is the leading cause of mortality worldwide. How such inflammation is initiated and maintained throughout the course of disease remains unclear. In the current study, we report the observation of specific phosphorylation of the receptor-interacting protein 3 (RIP3) kinase that marks the activation of programmed necrosis (also called the "necroptosis pathway") in the atherosclerotic plaques in apolipoprotein E (ApoE)-knockout mice. The mRNA expression levels of 10 inflammatory cytokines, including IL-1α, were decreased significantly in the plaque regions of mice lacking RIP3. Lymphocyte infiltrations in the adipocyte tissue and in skin lesions of ApoE single-knockout mice were significantly mitigated in ApoE/RIP3 double-knockout mice. The high percentage of inflammatory monocytes with high levels of lymphocyte antigen 6C in the blood of ApoE single-knockout mice also was greatly decreased in the ApoE/RIP3 double-knockout mice. Most significantly, the double-knockout mice displayed dramatically delayed mortality compared with ApoE single-knockout mice. Our findings indicate that necrotic death in areas such as atherosclerotic plaques may release cytokines that mobilize monocytes from bone marrow to the lesion sites, exacerbating the lesions in multiple tissues and resulting in the premature death of the animals.

necrosis | RIP3 | macrophages | atherosclerosis | longevity

Mouse models of cholesterol metabolism dysfunction such as apolipoprotein E (ApoE) knockout have been widely used to study atherosclerosis (1). Mice in which the *ApoE* gene is knocked out demonstrate severe phenotypes, with multiple plaques appearing on the aortic valve and arterial walls within a couple of months after starting a high-cholesterol diet (2). These mice also show chronic inflammation, and double knockout of ApoE and IL-1α resulted in reduced plaque areas (3–6).

A high level of lymphocyte antigen 6C ($Ly6C^{hi}$) is an inflammatory marker for atherosclerotic risk (7). In ApoE-deficient mice, the number of circulating $Ly6C^{hi}$ monocytes is increased (7). It has been hypothesized that these cells enter plaques more abundantly than $Ly6C^{low}$ monocytes (8). The monocytes subsequently differentiate into macrophages, which, after engulfing cholesterol crystals and becoming foam cells, die in situ to form the necrotic core of the plaques. These dead cells then send out damage-associated molecular patter (DAMP) signals to attract and mobilize more monocytes, completing a vicious cycle that accelerates disease progression (9).

Thus the particular mode of death of these macrophages—apoptosis or necrosis—can be a critical determinant for the initiation of inflammation, because necrotic death releases the cellular contents that constitute the DAMP signal to the blood stream, whereas apoptotic cell debris is engulfed by macrophages without leaking out of the cell (9).

Recently, the molecular mechanism of a form of programmed cell death termed "necroptosis" was characterized. This form of cell death can be triggered by the TNF family of cytokines and by ligands of Toll-like receptors 3 and 4 (10). The activated TNF receptor recruits receptor-interacting kinase 1 (RIP1) which in turn binds and activates a closely related kinase, RIP3, to form a necrosis-inducing protein complex (11). The activated RIP3 is marked by phosphorylation at the serine 227 site of human RIP3 (and at the equivalent serine 232 site of mouse RIP3) that allows it to bind and activate its downstream effector, a pseudokinase known as "mixed lineage kinase domain-like protein," MLKL (12). MLKL then is phosphorylated by RIP3 at the 357/358 sites (human) and the serine 345 site of mouse MLKL (13). The phosphorylated MLKL shifts into an oligomerized state that allows it to form membrane-disrupting pores, ultimately resulting in necrotic death (13).

After we developed a monoclonal antibody that specifically recognizes the phosphorylated serine 232 of mouse RIP3, we studied the role of necroptosis in atherosclerotic plaque areas by using this antibody to probe the signal of necroptosis activation. We further investigated the role of necroptosis in systematic inflammation by analyzing a panel of proinflammatory cytokines and immune cells in ApoE single-knockout and ApoE/RIP3 double-knockout mice. Finally, we addressed the consequences of necroptosis in the animals by comparing the lifespans of ApoE single-knockout and ApoE/RIP3 double-knockout mice fed either a high-cholesterol or a normal diet.

Results

To verify the specificity of rabbit monoclonal antibodies recognizing necroptosis-activating phosphorylation of RIP3 and MLKL, mouse bone marrow-derived macrophages (BMDMs) were induced to undergo necrosis by a combination of either TNF-α (T), Smac mimetic (S), and a pan-caspase inhibitor z-VAD-fmk (Z) (hereafter, TSZ) or the TLR4 ligand LPS plus zVAD (hereafter,

Significance

Atherosclerosis is one of the major causes of human death in modern society. A high blood cholesterol level resulting from cholesterol metabolism dysfunction is a key known contributing factor for premature atherosclerosis. Using a mouse model of high blood cholesterol, we show that a specific activation marker of a programmed necrosis mediated by the kinase receptor-interacting protein 3 (RIP3) can be detected in the core of atherosclerotic plaques. Mice lacking the *RIP3* gene showed a significant reduction of proinflammatory monocytes in the blood and delayed mortality. This study suggests that RIP3-mediated necrotic cell death is part of a self-amplifying proinflammatory cycle that contributes to the premature death of animals with the pro-atherosclerosis trait.

Author contributions: L.M., W.J., and X.W. designed research; L.M. and W.J. performed research; L.M. contributed new reagents/analytic tools; L.M., W.J., and X.W. analyzed data; and L.M. and X.W. wrote the paper.

Reviewers included: G.L., University of Texas Southwestern Medical Center.

The authors declare no conflict of interest.

Freely available online through the PNAS open access option.

[1]To whom correspondence should be addressed. Email: wangxiaodong@nibs.ac.cn.

This article contains supporting information online at www.pnas.org/lookup/suppl/doi:10.1073/pnas.1514730112/-/DCSupplemental.

LZ), as previously described (10, 11), and were analyzed by Western blotting using antibodies against phosphorylated serine 232 of mouse RIP3 and phosphorylated serine 345 of mouse MLKL. As shown in Fig. 1*A*, the cells treated with the vehicle DMSO alone did not show any signal (lanes 1 and 5). BMDMs from RIP3-knockout mice did not show any RIP3 protein or phosphorylation signals, as is consistent with a previous report that RIP3 kinase activity is required for necrosis induction by TNF-α/Smac (TS) mimetic and LPS after caspase activity is inhibited by the pan-caspase inhibitor z-VAD-fmk (TSZ and LZ) (10) (lanes 3 and 4 and lanes 7 and 8). In contrast, BMDMs from wild-type mice induced to undergo necroptosis by either the TSZ or the LZ combination showed robust RIP3 and MLKL phosphorylation signals (lanes 2 and 6). We detected no difference in the levels of GAPDH or of the inflammation protein NLRP3 in wild-type and RIP3-knockout BMDMs (lanes 1–8). The appearance of the phosphorylated RIP3 and MLKL signals was well correlated with cell survival as measured by intracellular ATP levels (Fig. 1*B*).

Because necroptosis is often accompanied by the release of proinflammatory cytokines (6), we used ELISA to test the release of IL-1α and IL-1β in the culture media of BMDMs. TS-induced apoptosis did not stimulate the release of IL-1α or IL-1β (Fig. S1 *A* and *B*). In contrast, necroptosis induction caused the release of both IL-1α and IL-1β, but these cytokines were close to the basal levels seen in normally growing cells when the BMDMs used for the treatment were from RIP3-knockout mice (Fig. 1 *C* and *D* and Fig. S1*C*). The BMDMs from MLKL-knockout mice behaved similarly to those from the RIP3-knockout mice, showing decreased release of IL-1α and IL-1β following treatment with TSZ and LZ (Fig. S1*A*). In comparison, medium from BMDMs treated with monosodium urate (MSU) crystals, which induce IL-1β secretion by activating nucleotide-binding domain, leucine-rich containing (NLR) family, pyrin domain containing 3 (NLRP3) inflammasomes (14), did not show any difference in the level of cytokine release in BMDMs derived from RIP3 wild-type or RIP3-knockout mice (Fig. S1*B*).

When fed a 1.25% high-cholesterol diet, the ApoE-deficient mice showed multiple atherosclerotic plaques on their aortic valves and aortas after 12, 16, and 20 wk of feeding (see Fig. S3 *A* and *B*). A typical plaque exhibited a large necrotic core and extracellular cholesterol clefts (15) as indicated by staining with Oil Red O and H&E (Fig. 2*A*). We used the monoclonal antibody that specifically recognizes the phosphorylated serine 232 site of mouse RIP3 to stain the plaques using immunohistochemical (IHC) methods. Unfortunately, the anti–phospho-MLKL antibody could not be used for IHC staining, because of nonspecific staining. As shown in Fig. 2*B*, in plaques from ApoE single-knockout mice, phosphorylated RIP3–stained brown dots were observed in the noncellular cavity areas that previously have been defined as the necrotic core (16). Quantification data for the stained dots of mice fed high-cholesterol diets for 16 wk are shown in Fig. 2*D*. Only weak background staining was seen in plaques from ApoE/RIP3 double-knockout mice (Fig. 2 *B* and *D*), and, as reported previously (17), the area of plaque in these mice was reduced compared with that in ApoE single-knockout mice (see Fig. S3 *A* and *B*). Interestingly, when the plaques were microdissected from aortic valve/aorta and analyzed by Western blotting, the plaques from ApoE single-knockout mice showed higher levels of RIP3 expression (lanes 4–9) than the plaques from wild-type mice (lanes 1–3) (Fig. 2*F*). No RIP3 signal was detected

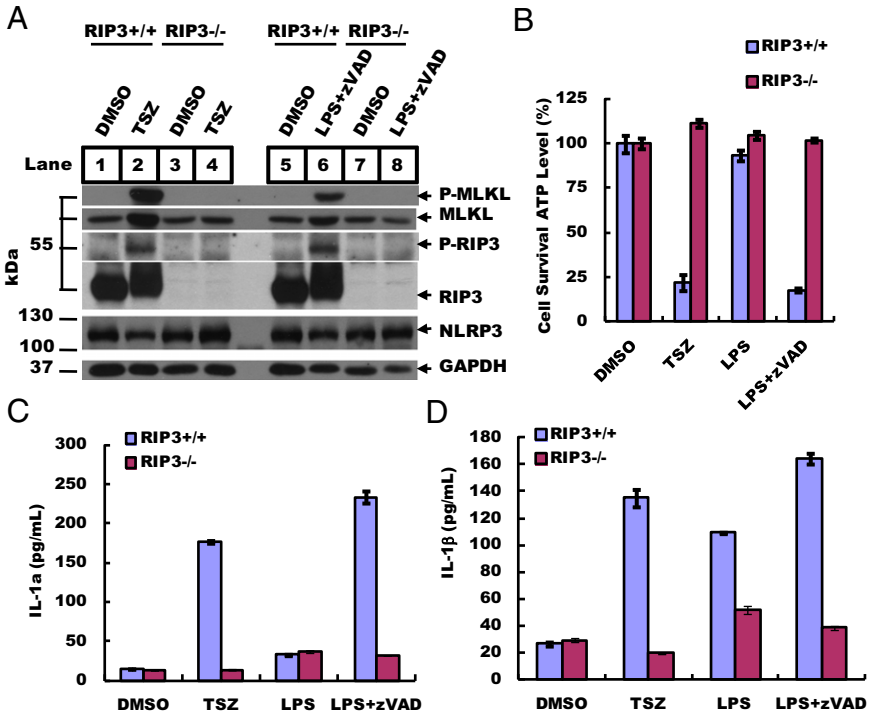

Fig. 1. RIP3 deletion suppresses necrosis and IL-1α/β production. (*A*) BMDMs from 8-wk-old RIP3$^{+/+}$ and RIP3$^{-/-}$ mice were treated with TSZ (20 ng/mL TNF-α, 100 nM Smac mimetic, and 20 μM zVAD) or LZ (20 ng/mL LPS and 20 μM zVAD) for 5 h. DMSO was used as a control. Cell lysates were collected, and sample aliquots were subjected to Western blot analysis of necrosis protein levels at the indicated conditions. Thirty micrograms of cell supernatant was loaded in each lane, except that 60 μg was loaded for phosphorylated RIP-3 (p-RIP3) and phosphorylated MLKL (p-MLKL). GAPDH is shown as a loading control. Blots were exposed to film at room temperature for 60 s. (*B*) BMDMs were treated at the indicated conditions for 12 h, and cell viability was determined by measuring ATP levels using a CellTiter Glo assay. Data represent the mean ± SD of duplicate samples. (*C* and *D*) BMDMs were cultured with different stimuli, as indicated, for 12 h. Secreted IL-1α and IL-1β levels were quantified by ELISA. All experiments were repeated at least three times with similar results.

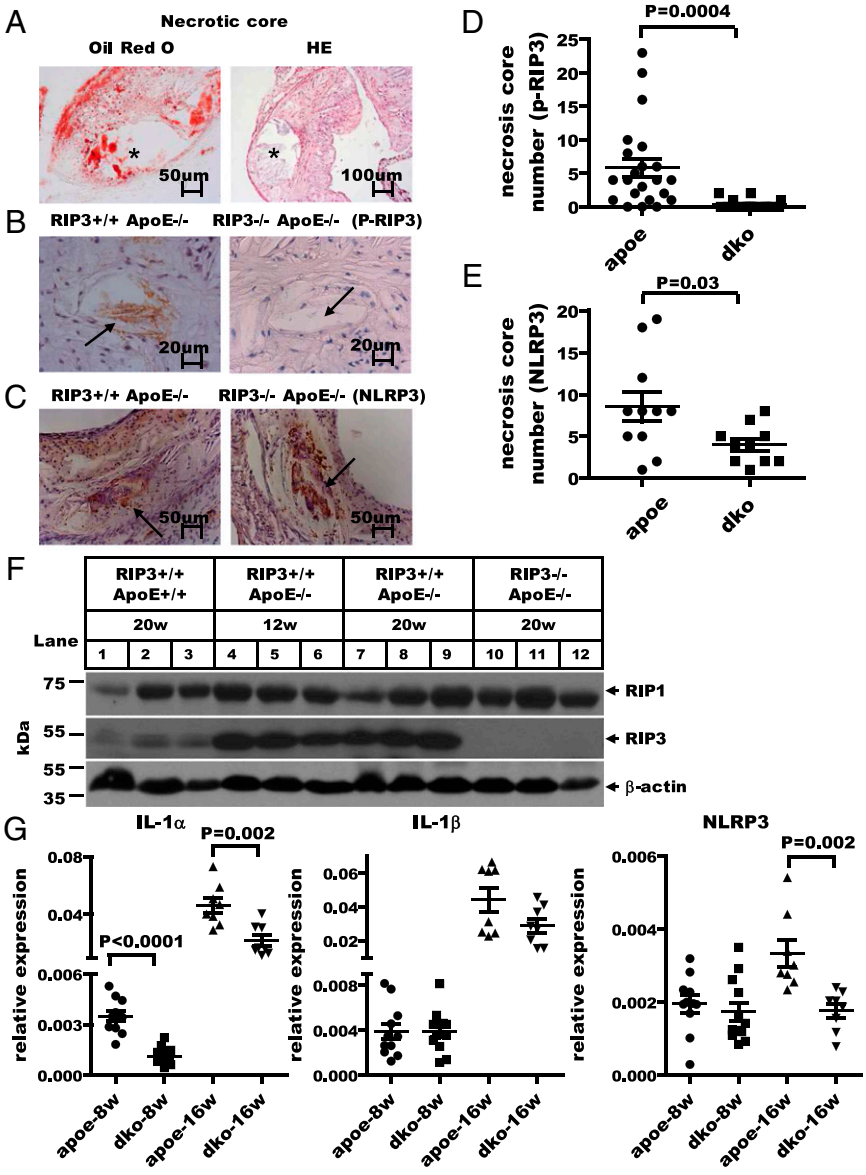

Fig. 2. RIP3 deletion suppresses inflammation in atherosclerotic plaques. (*A*) Cross-sections of typical atherosclerotic lesions exhibiting extensive staining with Oil Red O and H&E. The asterisk indicates the necrotic core. (*B*) Representative IHC staining of p-RIP3 in plaques from ApoE single-knockout and RIP3/ApoE double-knockout mice fed high-cholesterol diets (1.25%) for 16 wk. Positive-staining signals appear as brown dots in sections counterstained with hematoxylin (blue). Plaque staining of phosphorylated RIP3 is seen only in the necrotic core of ApoE single-knockout mice (black arrow). (*C*) IHC staining representative of NLRP3 expression in necrotic cores from ApoE single-knockout and RIP3/ApoE double-knockout mice fed high-cholesterol diets for 16 wk. The black arrows indicate necrotic cores with NLRP3 staining. (*D* and *E*) Quantitative data showing the number of necrotic cores stained by phosphorylated RIP3 ($n = 22$ ApoE single-knockout mice; $n = 20$ RIP3/ApoE double-knockout mice) and NLRP3 ($n = 11$ ApoE single-knockout mice; $n = 10$ RIP3/ApoE double-knockout mice). Vertical bars show the mean ± SD for each group. dko, double knockout. (*F*) Western blot analysis of RIP1 and RIP3 levels in plaque areas microdissected from aortic valves/aortas of wild-type and RIP3/ApoE double-knockout mice fed high-cholesterol diets for 20 wk ($n = 3$) and of ApoE single-knockout mice fed the same diet for 12 wk. β-Actin is shown as a loading control. An 60-μg aliquot of atherosclerotic plaque extracts was loaded in each lane. All experiments were repeated at least three times with similar results. (*G*) Microdissected atherosclerotic plaque from aortic valves/aortas of ApoE single-knockout and RIP3/ApoE double-knockout mice fed high-cholesterol diets for 8 or 16 wk; mRNA was extracted for quantitative RT-PCR analysis of the expression of the inflammatory genes *IL-1α*, *IL-1β*, and *NLRP3*. The gene-expression levels were normalized to the expression level of GAPDH. Data represent the mean ± SD. Unpaired Student's *t* tests were used to evaluate significance. A P value < 0.01 was considered significant.

in the plaques from RIP3-knockout mice, confirming the specificity of the antibody (lanes 10–12) (Fig. 2*F*). Stronger NLRP3 signals also were detected in atherosclerotic plaques of ApoE single-knockout mice than in plaques of ApoE/RIP3 double-knockout mice, suggesting that NLRP3 activity was augmented by the RIP3-mediated necroptosis pathway in the plaque areas (Fig. 2 *C* and *E*).

The other previously reported components of atherosclerotic lesions also were observed by immunofluorescence staining (18–20). Macrophage marker Mac-3 staining was observed on the inner edge of the plaque lining the luminal surface close to the vessel lumen (Fig. S2*A*). TUNEL staining was seen in the nonnuclear structures in atherosclerotic plaques (Fig. S2*A*). The apoptosis marker cleaved caspase-3 (21) was present in atherosclerotic plaque; it was located on the inside of the plaque close to the arterial wall (Fig. S2*A*). The areas stained by cleaved caspase-3 were apparently larger than the areas stained by phosphorylated RIP3 (Fig. S2*A*).

Consistent with a previous report (17), both the area and the thickness of the plaque in ApoE/RIP3 double-knockout mice were reduced compared with plaque in ApoE single-knockout mice (Fig. S3 *A* and *B*). Notably, the differences in the atherosclerotic plaques in mice with or without the *RIP3* gene were not caused by alterations in lipoprotein levels, because no differences were detected in the levels of very low-density lipoprotein, LDL, or HDL in the sera of ApoE single-knockout or ApoE/RIP3 double-knockout mice fed a high-cholesterol diet (Fig. S3*C*).

We extracted RNA from plaques in the aortic valve/aorta areas and performed quantitative real-time PCR analysis to evaluate the expression levels of a variety of proinflammatory cytokines. Plaques from ApoE/RIP3 double-knockout mice fed a high-cholesterol diet for 16 wk showed obviously reduced IL-1α (Fig. 2*G*, *Left*) mRNA levels compared with plaques from ApoE single-knockout mice. This trend also was observed for many additional cytokines, including IL-33, TNF-α, IL-2, intercellular adhesion molecule 1 (ICAM-1), TGF-β, Foxp3, Tbet, IL-17c, and IL-10 (Fig. S4). Furthermore, the expression of ICAM-1, a major adhesion molecule that plays a critical role in the homing of leukocytes to sites of atherosclerotic lesions, also was dramatically reduced in ApoE/RIP3 double-knockout mice (Fig. S4).

In addition to the plaques in aortic valves and aortas, ApoE single-knockout mice developed severe skin lesions (22, 23); these were most pronounced when mice were fed high-cholesterol diets for several weeks. Interestingly, the dull fur and extensive areas of alopecia at the interscapular area of skin observed in ApoE single-knockout mice appeared much less severe in the ApoE/RIP3 double-knockout mice (Fig. S5*A*). Histological analysis of skin revealed that ApoE/RIP3 double-knockout mice exhibited marked protection against skin thinning and ulcers, extracellular matrix degradation, and loss of dermal collagen density (Fig. S5*B*). Similarly, white adipose tissue of ApoE single-knockout mice fed a high-cholesterol diet for 16 wk had smaller adipocytes scattered with inflammatory granular cells; the granular cells were basically absent in ApoE/RIP3 double-knockout mice fed on the same diet and the size of adipocyte looked normal (Fig. S5*B*).

The local higher expression of the proinflammatory cytokines in the atherosclerotic plaques potentially can mobilize monocytes from bone marrow to these sites (24–26). One such event can be measured by monitoring the level of the Ly6C marker in circulating monocytes in blood. This marker has been shown to be elevated in hypercholesterolemia-associated monocytes in mice and is known to give rise to the macrophages in atherosclerotic lesions (7, 27). Therefore we isolated cells from mouse blood and stained samples with the following antibodies: CD4, CD8, CD19, NK1.1, CD11c, CD11b, Ly6C, or Ly6G. The populations of lymphocytes, natural killer (NK) cells, dendritic cells (DCs), neutrophils, eosinophils, Ly6C^{hi} monocytes, and Ly6C^{low} monocytes were analyzed according to procedures described previously (28).

Blood monocyte subsets were discriminated by flow cytometry, and cells were gated on a discernable scatter population that contained all CD11c cells. The CD11c^{+}-CD11b^{+} monocyte population then was analyzed for Ly6C and Ly6G expression. Three discrete populations of monocytes were identified, expressing high, intermediate, and low levels of the marker Ly6C, respectively (28).

In agreement with previous reports, starting from 4 wk of high-cholesterol diet feeding, we observed a shift toward the CD11b^{+}Ly6C^{hi} subset in the blood of ApoE single-knockout mice compared with wild-type mice (Fig. 3*A*). The percentage of inflammatory monocytes in ApoE/RIP3 double-knockout male mice remained in the 3–4% range, compared with 4–9% of the ApoE single-knockout male mice as the disease progressed from week 4 to week 15 on a high-cholesterol diet (Fig. 3*A*). We also measured the percentage of Ly6C^{hi} monocytes in the blood of female ApoE single-knockout and ApoE/RIP3 double-knockout mice fed a high-cholesterol diet for 4, 8, 12, and 16 wk.

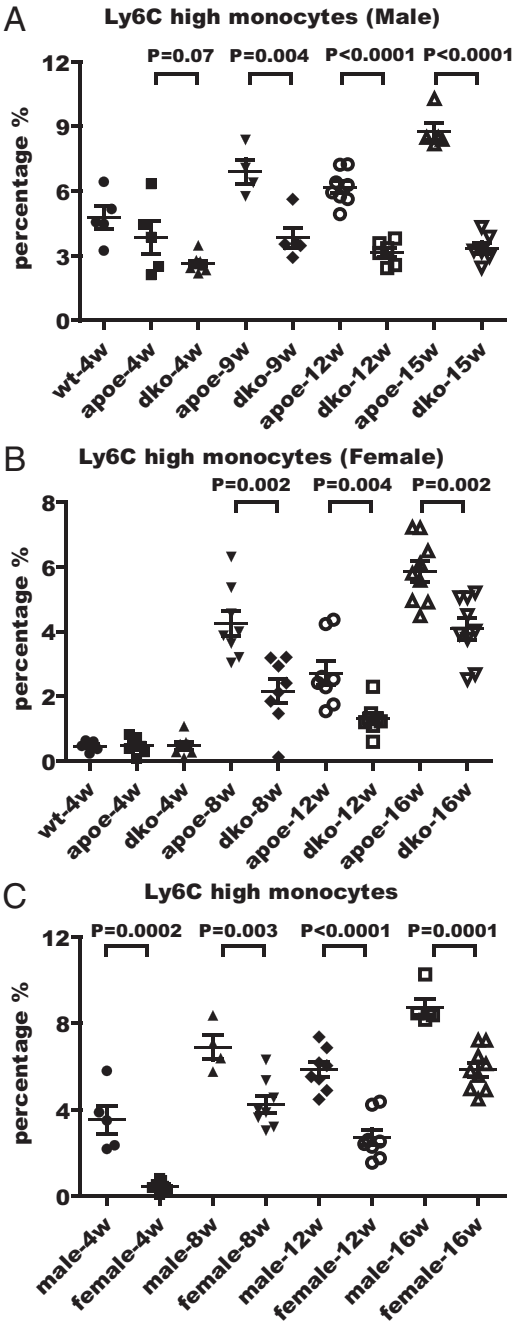

Fig. 3. Deletion of RIP3 decreases the percentage of Ly6C^{hi} inflammatory monocytes in blood during the progression of atherosclerotic disease. (*A* and *B*) Flow cytometry analysis of the percentage of the inflammatory monocyte population in the blood of male (*A*) and female (*B*) mice at the indicated times after high-cholesterol diet feeding. wt, wild type; apoe, ApoE single-knockout mice; dko, ApoE/RIP3 double-knockout mice. Cells were stained with antibodies against CD4, CD8, CD19, NK1.1, CD11c, CD11b, Ly6C, and Ly6G and were processed as described in *Materials and Methods*. (*C*) Comparison of the percentage of Ly6C^{hi} inflammatory monocytes in male and female ApoE single-knockout mice.

Similar to the results in male mice, female RIP3/ApoE double-knockout mice showed a decreased percentage of Ly6C^{hi} monocytes compared with the ApoE single-knockout mice at each time point (Fig. 3*B*). The percentage of Ly6C^{hi} monocytes is significantly lower in female mice than in male mice fed the same high-cholesterol diet (Fig. 3*C*). However, no differences in

the percentage of NK cells, DCs, neutrophils, or eosinophils were detected between male and female mice (Fig. S6).

Finally, we compared the lifespans of ApoE single-knockout and RIP3/ApoE double-knockout mice. As can be seen from the Kaplan–Meier curves in Fig. 4, the survival of the double-knockout mice was significantly higher than that of the ApoE single-knockout mice. The ApoE single-knockout male mice started to die at 7 wk on the high-cholesterol diet, and 50% of the cohort was dead by ∼6.5 mo (26 wk) on the high-cholesterol diet. The median survival of the double-knockout male mice on the same diet was 8.25 mo (33 wk) ($P < 0.001$) (Fig. 4*A*). The ApoE single-knockout female mice did not start to die until they had been on a high-cholesterol diet for 15 wk and had a median survival time of ∼8 mo (32 wk). For female double-knockout mice the protective effect was even more pronounced at younger ages, with a median survival of 10.25 mo (41.5 wk) ($P < 0.001$) (Fig. 4*B*), a more than 2-mo delay of mortality compared with the ApoE single-knockout female mice.

Even on normal chow diet, the survival rate of the double-knockout mice was significantly higher than that of the ApoE single-gene knockout mice, although the death rate was significantly lower than that of mice on a high-cholesterol diet (Fig. 4 *C* and *D*). At 21 mo of age, when 50% of ApoE single-knockout male mice had died, 88% of the double-knockout male mice were still alive ($P < 0.001$) (Fig. 4*C*). For female mice, 50% of the ApoE -knockout mice died by ∼11.5 mo of age, compared with 17 mo for the double-knockout mice ($P < 0.001$) (Fig. 4*D*). Interestingly, the female mice on the normal chow diet actually died faster than male mice, whereas females on a high-cholesterol diet were more protected than males. The percentages of Ly6C^{hi} monocytes correlated with the mortality rates (Fig. 3*C*), but the levels of estradiol and progesterone were similar in female single- and double-knockout mice and apparently did not contribute to the observed difference in their mortality (Fig. S7).

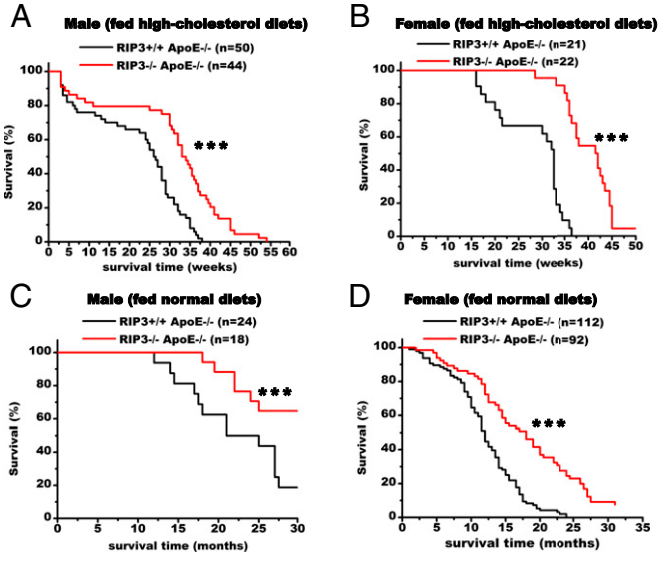

Fig. 4. Deletion of RIP3 prolongs the lifespan of the atherosclerotic mice. (*A* and *B*) Comparison of survival of ApoE single-knockout and RIP3/ApoE double-knockout male (*A*) and female (*B*) mice. Survival curves start with 8-wk-old mice fed high-cholesterol diets (1.25%). ApoE single-knockout mice exhibited significantly decreased survival relative to RIP3/ApoE double-knockout mice. (*C* and *D*) Survival curves of ApoE single-knockout and RIP3/ApoE double-knockout male (*C*) and female (*D*) mice fed normal diets and recorded age at death. Data were analyzed with Kaplan–Meier tests. Asterisks denote the level of statistical significance between ApoE single-knockout and RIP3/ApoE double-knockout male and female mice: ***$P < 0.001$.

Discussion

High blood cholesterol and systematic inflammation have long been implicated in cardiovascular diseases (1), and how these two factors interplay during the initiation and progression of the disease has been a longstanding question. The study described here used a mouse model of high blood cholesterol and defects in programmed necrosis to address the interplay of high blood cholesterol and systematic inflammation. It is clear that high blood cholesterol in the ApoE single-knockout mice is sufficient to cause atherosclerotic plaque formation, even without the systematic inflammation contributed by RIP3-mediated necrosis. However, disease progression, as measured by plaque area and thickness, was significantly slowed in the absence of necroptosis.

We believe this slowing of disease progression results from an interruption of the vicious cycle of necroptosis-induced inflammation in lesion sites such as atherosclerotic plaques. An antibody that specifically recognizes phosphorylated serine 232, which marks the activation of RIP3, stained positively at the plaque cores. The expression levels of 10 proinflammatory cytokines, including IL-1α, in the atherosclerosis plaques were lower in the absence of RIP3. These cytokines may contribute to the mobilization of activated inflammation Ly6C^{hi} monocytes from bone marrow, which enter into the lesion sites, differentiate into macrophages, and die in situ through necroptosis.

The most interesting result from this study is that mice without RIP3-mediated cell death not only manifested much less severe lesions in multiple tissues but also had significantly delayed mortality. This longevity effect is independent of sex and diet. It also is worth noting that when fed a high-cholesterol diet, young female mice were more protected than young males, similar to observations in humans (29).

What causes necroptosis in the atherosclerotic plaques remains to be determined. It is likely that cholesterol crystals and local higher concentrations of inflammatory cytokines contribute to the death of macrophages. Also, how different diets cause different responses in male and female mice is an interesting topic for future research.

Nevertheless, by using the small molecules specifically targeting necroptosis, which are being developed, it should be possible to alleviate the symptoms and prolong the lives of patients suffering from atherosclerosis.

Materials and Methods

Mice. The research involving animals have been approved by the institutional review board of National Institute of Biological Sciences, Beijing. ApoE single-knockout mice (C57BL/6 background) were originally from Jackson Laboratories. RIP3$^{-/-}$ mice were back-crossed for 10 generations into the C57BL6/J strain generated in our Transgenic Research Center in the National Institute of Biological Science. Mice were matched for age and sex and were used for experiments when 8 wk old. The doubly heterozygous progeny were intercrossed to generate double-knockout ApoE$^{-/-}$RIP3$^{-/-}$ mice and ApoE single-knockout ApoE$^{-/-}$RIP3$^{+/+}$ mice. At 8 wk of age, ApoE$^{-/-}$RIP3$^{-/-}$ or sex-matched ApoE$^{-/-}$RIP3$^{+/+}$ mice were placed on a high-cholesterol diet (40 kcal% fat, 1.25% cholesterol, 0.5% cholic acid; Research Diets, Inc. no. D12109). The first day mice were fed this diet was defined as day 0 in this study. The remaining animals consumed a regular chow diet.

Atherosclerosis Experiments. Quantification of atherosclerotic lesions was performed as described previously (15). The OCT-embedded frozen sections were cut serially through the aorta at the origins of the aortic valve leaflets, and every fifth section (7-μm interval) from the aortic sinus was mounted on slides for measurement of plaque area and for IHC staining. Sections were stained with Oil Red O for analysis of the lesion area. Tissues were fixed in 10% (vol/vol) phosphate-buffered formalin, embedded in paraffin, and histological sections were stained with H&E for pathological analysis. Images were analyzed using ImageJ software. For IHC and immunofluorescence staining, plaque sections were washed with PBS and then were fixed with 4% (vol/vol) paraformaldehyde for 15 min at room temperature. Sections then were incubated in 0.1% Triton X-100 (Sigma) in PBS for 15 min at room temperature. After two washings with PBS, sections were blocked in a solution

of PBS containing 5% (vol/vol) goat serum for 2 h at 4 °C. Primary and secondary antibodies were diluted in a solution of PBS containing 5% (vol/vol) goat serum overnight. Following a third washing with PBS, slides were qualitatively examined for 3,3′-diaminobenzidine-tetrahydrochloride (DAB) staining (brown). The number of regions with positive staining for the phosphorylated RIP3 antibody was counted. Images were captured with an AxioCam MRc5 camera and a Carl Zeiss light microscope using Axiovision Software.

BMDM Culture. BMDMs were harvested from the bone marrow of both tibias of 8-wk-old male mice. Cells were collected by inserting a needle into the bone and were washed with DMEM supplemented with 1% L-glutamine, 1% penicillin/streptomycin, 20% (vol/vol) FBS, and 30% (vol/vol) L929 conditioned medium. This culture medium was refreshed (10 mL) once every 2 d. Bone marrow myeloid progenitor cells were differentiated into BMDMs for 5–7 d in L929 conditioned medium (37 °C, 5% CO_2). After differentiation, BMDMs were gently pipetted in cold 1× PBS and replated in 96-well plates at 1×10^4 cells per well in 1640 complete medium for cell death ATP level assays or in six-well plates at 2×10^6 cells per well for ELISA and Western blotting. BMDMs were stimulated for 5 h in the indicated condition for Western blot analysis protein expression. BMDMs were stimulated for 12 h for cell death assays by Cell-Titer Glo assay. BMDMs were stimulated for 12 h to collect cell supernatant for ELISA assay (IL-1α and IL-1β; R&D systems). BMDMs were treated with TNF-α (20 ng/mL), Smac (100 nM), zVAD (20 μM) (TSZ) or with LPS (20 ng/mL) or poly (I:C) (1 μg/mL) and zVAD to induce necrotic cell death. For inflammasome activation BMDMs were treated with LPS (20 ng/mL) for 24 h followed by ATP (5 mM) or MSU (300 μg/mL) for 12 h.

Antibodies and Reagents. The Smac mimetic compound, zVAD, and TNF-α were produced as described (11). LPS (L3012) and ATP (A6419) were from Sigma; poly (I:C) (31852-29-6) was from InvivoGen; MSU (AG-CR1-3950-2002) was from Adipogen. The ELISA kits were all from R&D Systems and included IL-1α (MLA00) and IL-1β (MLB00C). The following antibodies were used for experiments: cleaved caspase-3 (#9661, 1:200) and RIP1 (#3493, 1:200) from Cell Signaling; anti–Mac-3 (550292, 1:200) from BD; anti–β-actin HRP (PM053-7) and anti-GAPDH (M171-7) from MBL (1:5,000); anti-RIP3 (AHP1797; 1:1,000 for Western blotting) from AbD Serotec; anti-NLRP3 (1:200 for IHC, 1:1,000 for Western blotting) from the laboratory of Feng Shao, National Institute of Biological Sciences, Beijing; anti-pRIP3 and anti-pMLKL (1:200 for IHC, 1:1,000 for Western blotting) were generated in collaboration with Abcam.

Real-Time PCR. Total RNA from plaque in the aortic valves and aortas of mice was prepared using TRIzol reagent (Invitrogen). RNA samples were used to synthesize cDNA using a QuantiTect Reverse Transcription kit (Takara). Each reaction was prepared with SYBR Green (Takara) according to the manufacturer's instructions. The following primers were used: mIL-1a, 5′-AGCGCTCAAGGAGAAGACC-3′ and 5′-CCAGAAGAAAATGAGGTCGG-3′; mIL-1b, 5′-TGTGAAATGCCACCTTTTGA-3′ and 5′-GGTCAAAGGTTTGGAAGCAG-3′; mNLRP3, 5′-ATTACCCGCCCGAGAAAGG-3′ and 5′-TCGCAGCAAAGATCCACACAG-3′; mGAPDH, 5′-CTCATGACCACAGTCCATGCCATC-3′ and 5′-CTGCTTCACCACCTTCTTGATGTC-3′. Analysis of gene expression was performed using the comparative CT method. The expression level of each gene was normalized to the expression level of GAPDH using the standard curve method.

Flow Cytometry Analysis. Leukocytes were isolated from whole blood and subjected to red blood lysis. After washing, cells were blocked with anti-mouse CD16/CD32 antibody and then stained with the various antibodies for FACS analysis. Fluorophore-conjugated antibodies were purchased from BD Biosciences and eBioscience. The following monoclonal antibodies were used for flow cytometric cell marker analysis: CD4, CD8, CD19 (each 1:400), NK1.1, CD11c, CD11b, Ly6C, and Ly6G (each 1:200). Side-scatter and forward-scatter profiles were used to eliminate debris and cell doublets. Stained cells were analyzed using an LSRII flow cytometer (BD Biosciences). Data were analyzed using FlowJo software (Tree Star).

Statistical Analysis. Prism software (GraphPad Prism 5) was used for statistical analysis. Data were assessed using two-tailed Student's *t* tests (paired or unpaired, as appropriate) and two-way ANOVA with post hoc Bonferroni testing to assess progressive changes between groups. All probabilities are two-sided, and a value of $P < 0.05$ was considered statistically significant.

ACKNOWLEDGMENTS. We thank Dr. Liping Zhao (Harvard Medical School) for generating the ApoE$^{-/-}$RIP3$^{-/-}$ mice and critically reading the manuscript; Professor Chen Dong (Tsinghua University) for expert help and critically reading the manuscript; Ms. Yuqiong Liang (Salk Institute For Biological Studies) for expert help with immunological techniques; Dr. Yuhui Wang (Peking University) for providing ApoE single-knockout mice; and Cai Zhang, Mi Lian, Le Yin, Yongfen Ma, Xiao Liu, and Huanwei Huang for technical assistance. This work was supported by National Basic Science 973 Grants 2010CB835400, 2012CB837400, and 2013CB530805 from the Chinese Ministry of Science and Technology and by the Beijing Municipal Commission of Science and Technology.

1. Libby P (2002) Inflammation in atherosclerosis. *Nature* 420(6917):868–874.
2. Breslow JL (1996) Mouse models of atherosclerosis. *Science* 272(5262):685–688.
3. Cohen I, et al. (2010) Differential release of chromatin-bound IL-1alpha discriminates between necrotic and apoptotic cell death by the ability to induce sterile inflammation. *Proc Natl Acad Sci USA* 107(6):2574–2579.
4. Thorp E, et al. (2009) Reduced apoptosis and plaque necrosis in advanced atherosclerotic lesions of Apoe-/- and Ldlr-/- mice lacking CHOP. *Cell Metab* 9(5):474–481.
5. Kamari Y, et al. (2011) Reduced atherosclerosis and inflammatory cytokines in apolipoprotein-E-deficient mice lacking bone marrow-derived interleukin-1α. *Biochem Biophys Res Commun* 405(2):197–203.
6. Elkon KB (2007) IL-1alpha responds to necrotic cell death. *Nat Med* 13(7):778–780.
7. Swirski FK, et al. (2007) Ly-6Chi monocytes dominate hypercholesterolemia-associated monocytosis and give rise to macrophages in atheromata. *J Clin Invest* 117(1):195–205.
8. Combadière C, et al. (2008) Combined inhibition of CCL2, CX3CR1, and CCR5 abrogates Ly6C(hi) and Ly6C(lo) monocytosis and almost abolishes atherosclerosis in hypercholesterolemic mice. *Circulation* 117(13):1649–1657.
9. Edye ME, Lopez-Castejon G, Allan SM, Brough D (2013) Acidosis drives damage-associated molecular pattern (DAMP)-induced interleukin-1 secretion via a caspase-1-independent pathway. *J Biol Chem* 288(42):30485–30494.
10. He S, Liang Y, Shao F, Wang X (2011) Toll-like receptors activate programmed necrosis in macrophages through a receptor-interacting kinase-3-mediated pathway. *Proc Natl Acad Sci USA* 108(50):20054–20059.
11. He S, et al. (2009) Receptor interacting protein kinase-3 determines cellular necrotic response to TNF-alpha. *Cell* 137(6):1100–1111.
12. Sun L, et al. (2011) Mixed lineage kinase domain-like protein mediates necrosis signaling downstream of RIP3 kinase. *Cell* 148(1-2):213–227.
13. Wang H, et al. (2014) Mixed lineage kinase domain-like protein MLKL causes necrotic membrane disruption upon phosphorylation by RIP3. *Mol Cell* 54(1):133–146.
14. Duewell P, et al. (2010) NLRP3 inflammasomes are required for atherogenesis and activated by cholesterol crystals. *Nature* 464(7293):1357–1361.
15. Björkbacka H, et al. (2004) Reduced atherosclerosis in MyD88-null mice links elevated serum cholesterol levels to activation of innate immunity signaling pathways. *Nat Med* 10(4):416–421.
16. Seimon T, Tabas I (2009) Mechanisms and consequences of macrophage apoptosis in atherosclerosis. *J Lipid Res* 50(Suppl):S382–S387.
17. Lin J, et al. (2013) A role of RIP3-mediated macrophage necrosis in atherosclerosis development. *Cell Reports* 3(1):200–210.
18. Swirski FK, et al. (2006) Monocyte accumulation in mouse atherogenesis is progressive and proportional to extent of disease. *Proc Natl Acad Sci USA* 103(27):10340–10345.
19. Shalhoub J, Falck-Hansen MA, Davies AH, Monaco C (2011) Innate immunity and monocyte-macrophage activation in atherosclerosis. *J Inflamm (Lond)* 8:9.
20. Gui T, Shimokado A, Sun Y, Akasaka T, Muragaki Y (2012) Diverse roles of macrophages in atherosclerosis: From inflammatory biology to biomarker discovery. *Mediators Inflamm* 2012:693083.
21. Suzuki A, Iwasaki M, Wagai N (1997) Involvement of cytoplasmic serine proteinase and CPP32 subfamily in the molecular machinery of caspase 3 activation during Fas-mediated apoptosis. *Exp Cell Res* 233(1):48–55.
22. Libby P, Ridker PM, Hansson GK; Leducq Transatlantic Network on Atherothrombosis (2009) Inflammation in atherosclerosis: From pathophysiology to practice. *J Am Coll Cardiol* 54(23):2129–2138.
23. Hansson GK, Klareskog L (2011) Pulling down the plug on atherosclerosis: Cooling down the inflammasome. *Nat Med* 17(7):790–791.
24. Tacke F, et al. (2007) Monocyte subsets differentially employ CCR2, CCR5, and CX3CR1 to accumulate within atherosclerotic plaques. *J Clin Invest* 117(1):185–194.
25. Tsou CL, et al. (2007) Critical roles for CCR2 and MCP-3 in monocyte mobilization from bone marrow and recruitment to inflammatory sites. *J Clin Invest* 117(4):902–909.
26. Auffray C, et al. (2007) Monitoring of blood vessels and tissues by a population of monocytes with patrolling behavior. *Science* 317(5838):666–670.
27. Mildner A, et al. (2007) Microglia in the adult brain arise from Ly-6ChiCCR2+ monocytes only under defined host conditions. *Nat Neurosci* 10(12):1544–1553.
28. Rose S, Misharin A, Perlman H (2012) A novel Ly6C/Ly6G-based strategy to analyze the mouse splenic myeloid compartment. *Cytometry A* 81(4):343–350.
29. Pettersson US, Waldén TB, Carlsson PO, Jansson L, Phillipson M (2012) Female mice are protected against high-fat diet induced metabolic syndrome and increase the regulatory T cell population in adipose tissue. *PLoS One* 7(9):e46057.